# Supporting Information

## Sahoo et al. 10.1073/pnas.1313247110

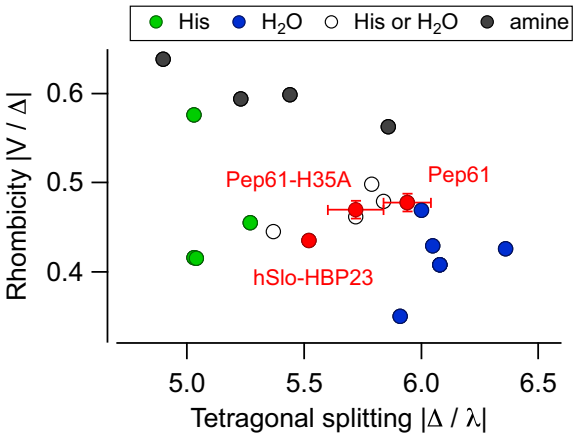


**Fig. S1.** Classification of hemin-binding modes based on electron paramagnetic resonance (EPR) signals. The X-band EPR spectra of peptide encoding the first 61 residues of Kv1.4 (Pep61) and Pep61-H35A with hemin displayed the typical rhombic signals of a low-spin ferric heme (Fig. 4D). The observed *g* values are similar to those of a series of ferric heme systems with cysteine thiolate as one of the axial ligands at the iron center (Table S1). A useful method to identify the axial ligand pattern is the ligand field analysis of the *g* values. The resulting plot of rhombicity ($|V/\Delta|$) vs. the tetragonality ($|\Delta/\lambda|$) of ferric heme systems (V, rhombic splitting parameter; $\Delta$, tetragonal splitting parameter; $\lambda$, spin-orbit coupling) can be used to identify specific areas for particular ligand patterns. In this graph, displaying our measurements and literature values from systems with cysteine thiolate as one of the axial ligands at the iron center (Table S1), the red symbols indicate values for the heme-binding peptide from the Slo1 BK channel (hSlo-HBP23)1, Pep61, and Pep61-H35A, the latter two from this study. From this plot it is evident that the second ligand for hSlo-HBP23 cannot unambiguously be assigned because the parameters for the hSlo-HBP23 heme adduct are at the borderline between the areas for histidine and H2O/OH– as the second axial ligand. The same is true for Pep61 and Pep61-H35A, which are also between Cys/$H_2O$ and Cys/His ligation. In both cases, the EPR signals are compatible with Cys acting as fifth ligand and a sandwich His/His ligation can be excluded.

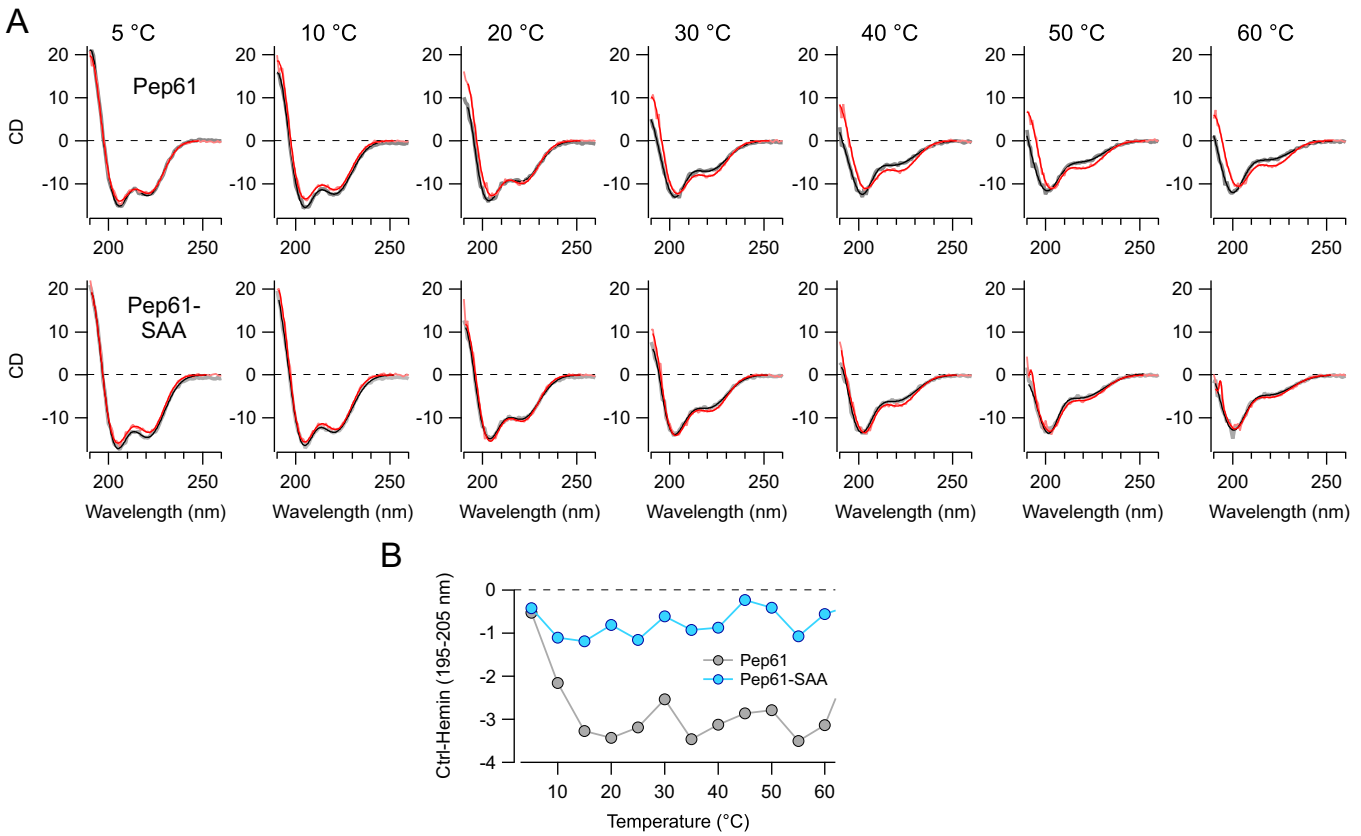


**Fig. S2.** Temperature dependence of Pep61 circular dichroism (CD) spectra. (*A*) CD spectra of Pep61 (*Upper*) and Pep61-C13S:H16A:A23W:H35A (SAA) (*Lower*) without (black) and with hemin (red) for the indicated temperatures. Peptide concentration was 12.5 μM and hemin at 50 μM. (*B*) Difference in CD spectra between 195 and 205 nm, indicative of changes in the content of random coil and β -sheet components, before and after hemin application as a function of temperature, illustrating that hemin has a consistently smaller impact on structural parameters on the mutant compared with the WT.

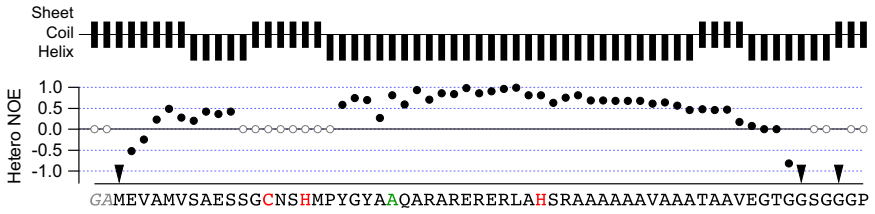


**Fig. S3.** NMR analysis of Pep61. Chemical shift index (CSI; *Top*) and steady-state backbone $^{15}N\{^{1}H\}$-nuclear Overhauser enhancement effect (NOE) (*Middle*), with primary structure of Pep61 (*Bottom*). Arrows indicate residues with heteronuclear NOE values below –1.0. Open circles indicate residues for which mobility could not be determined owing to signal overlap. In the sequence, cloning overhangs are shown in italics, and numbering starts with M1. C13, H16, A23, and H35 are highlighted. The CSI (1) allows to locate secondary structure elements in proteins based on the $^{1}H^{\alpha}$, $^{13}C^{\alpha}$, $^{13}C^{\beta}$, and $^{13}C'$ chemical shifts without recourse to distance (NOE) data. An elongated central α-helical element between residues P18 and A47, as well as two shorter α-helical segments N- and C-terminal to it (S7–S11, E52–G58), are predicted. The assessment of the peptide's dynamics by means of the heteronuclear NOEs consistently shows a low mobility for the segment 18–46 for which an alpha-helical (α) helical conformation is predicted.

1. Wishart DS, Sykes BD (1994) The 13C chemical-shift index: A simple method for the identification of protein secondary structure using 13C chemical-shift data. *J Biomol NMR* 4(2): 171–180.

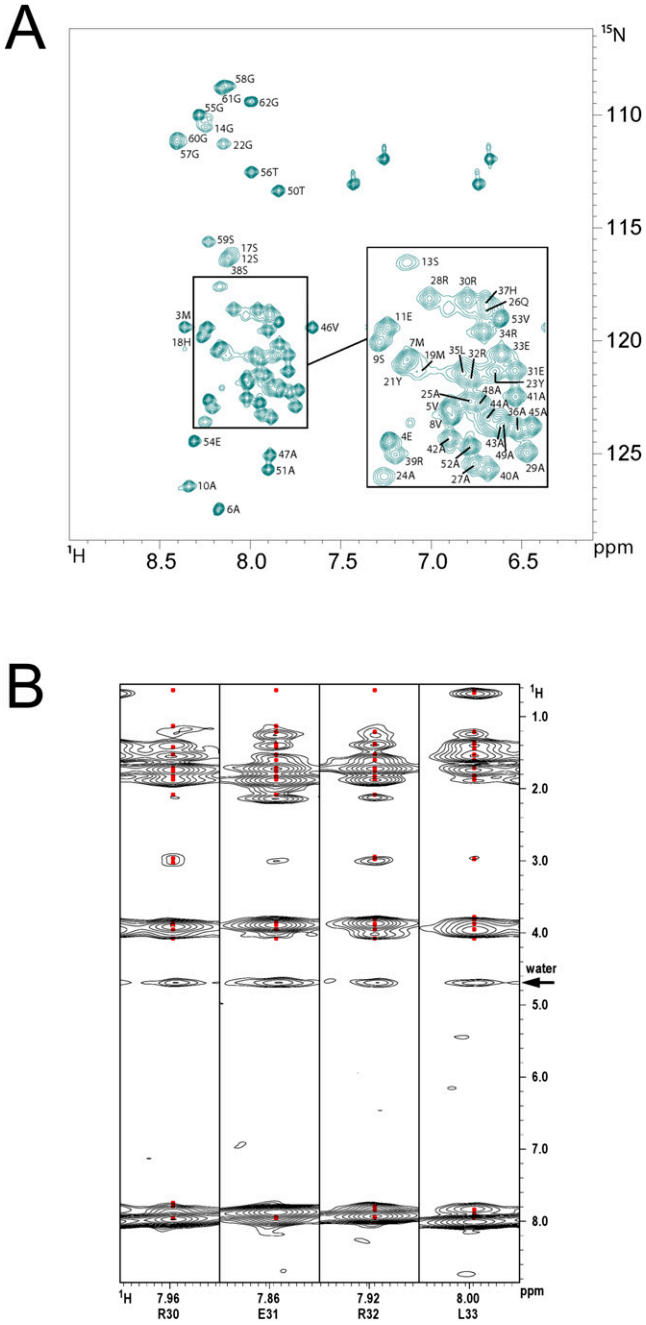


**Fig. S4.** Representative NMR spectra. (*A*) [$^{1}$H,$^{15}$N]-HSQC spectrum of Pep61. Backbone amide resonance assignments are indicated by residue number followed by the one-letter code of the amino acid type. (*B*) Strips of the [$^{1}$H,$^{1}$H,$^{15}$N]-nuclear Overhauser enhancement spectroscopy (NOESY)-heteronuclear single quantum coherence (HSQC) spectrum of Pep61. The stretch R30–L33 is shown. Red dots indicate the positions of cross peaks predicted for the starting structure of the heme docking generated with a distance range of 5 Å. Diagonal peaks are omitted. The good coincidence of the experimental NOE cross-peaks and the predicted peak positions supports the validity of the starting structure for the subsequent docking.

**Table S1. EPR and ligand field parameters for low-spin ferric heme proteins with thiolate ligation**

| Protein | Iron ligands | $g_1$ | $g_2$ | $g_3$ | $\lvert\Delta/\lambda\rvert$ | $\lvert V/\Delta\rvert$ | Reference |
|---|---|---|---|---|---|---|---|
| Kv1.4-IP (Pep61) + hemin | | 2.46 | 2.26 | 1.91 | 5.94 | 0.478 | This work |
| Kv1.4-IP (Pep61-H35A) + hemin | | 2.47 | 2.27 | 1.90 | 5.72 | 0.462 | This work |
| hSlo-HBP23 + hemin | | 2.72 | 2.51 | 2.08 | 5.52 | 0.435 | (1) |
| HRI | Cys/His | 2.49 | 2.28 | 1.87 | 5.27 | 0.455 | (2) |
| Δ145 HRI | Cys/$H_2O$ | 2.42 | 2.26 | 1.91 | 6.08 | 0.408 | (3) |
| HRI-KI | Cys/$H_2O$ | 2.43 | 2.26 | 1.91 | 6.05 | 0.429 | (4) |
| CBS | Cys/His | 2.5 | 2.3 | 1.86 | 5.03 | 0.416 | (5) |
| H450, pH 8 | Cys/$H_2O$ | 2.42 | 2.28 | 1.91 | 5.91 | 0.350 | (6) |
| H450, pH 6 | Cys/His | 2.51 | 2.31 | 1.87 | 5.04 | 0.415 | (6) |
| CooA, *Escherichia coli* | Cys/His, $H_2O$ | 2.46 | 2.25 | 1.89 | 5.79 | 0.498 | (7) |
| CooA, *Rhodospirillum rubrum* | Cys/His, $H_2O$ | 2.46 | 2.26 | 1.90 | 5.84 | 0.479 | (8) |
| P450 RLM-PB | Cys/$H_2O$ | 2.41 | 2.25 | 1.92 | 6.36 | 0.426 | (9) |
| P450 MIT | Cys/$H_2O$ | 2.42 | 2.26 | 1.91 | 6.08 | 0.408 | (10) |
| P450 PP-CAM | Cys/$H_2O$ | 2.45 | 2.26 | 1.91 | 6.00 | 0.469 | (11) |
| P450 RLM-PB + *N*-MeIm | Cys/*N*-MeIm | 2.54 | 2.26 | 1.88 | 5.44 | 0.599 | (9) |
| P450 RLM-PB + *n*-octylamine | Cys/amine | 2.49 | 2.25 | 1.90 | 5.86 | 0.563 | (9) |
| P450 PP-CAM + Im | Cys/Im | 2.56 | 2.27 | 1.87 | 5.23 | 0.594 | (11) |
| P450 PP-CAM + 2-MeIm | Cys/2-MeIm | 2.62 | 2.28 | 1.85 | 4.90 | 0.639 | (11) |
| cyt *c*-M80C | Cys/His | 2.56 | 2.27 | 1.85 | 5.03 | 0.576 | (7) |
| IRP2 | Cys/His, $H_2O$ | 2.47 | 2.27 | 1.87 | 5.37 | 0.445 | (12) |

$g_1$, $g_2$, $g_3$, *g* factors or Landé factors; HRI, heme-regulated inhibitor kinase; hSlo-HBP23, 23-residue peptide encompassing the heme-binding segment; H450, purified from rat liver cytosol; Im, imidazole; IRP2, Iron regulatory protein 2; Kv1.4-IP, synthetic or recombinant inactivation peptide of potassium channel Kv1.4, encompassing the first 61 residues; *N*-MeIm, *N*-methylimidazole; P450 RLM-PB, rat liver microsomal cytochrome P450 induced by phenobarbitone; P450 MIT, cytochrome P450 in bovine adrenal cortex submitochondrial particles; P450 PP-CAM, cytochrome P450 from *Pseudomonas putida* grown on D-campher; Δ145 HRI, N-terminal truncated mutant; HRI-KI, isolated kinase insertion domain; CBS, human cystathionine β-synthase; $\lvert\Delta/\lambda\rvert$, tetragonal splitting of the ligand field in units of γ (Δ, tetragonal splitting parameter; λ, spin-orbit coupling); $\lvert V/\Delta\rvert$, rhombicity of the ligand field (*V*, rhombic splitting parameter; Δ, tetragonal splitting parameter); 2-MeIm, 2-methylimidazole.


1. Tang XD, et al. (2003) Haem can bind to and inhibit mammalian calcium-dependent Slo1 BK channels. *Nature* 425(6957):531–535.
2. Igarashi J, et al. (2004) Activation of heme-regulated eukaryotic initiation factor 2α kinase by nitric oxide is induced by the formation of a five-coordinate NO-heme complex: Optical absorption, electron spin resonance, and resonance raman spectral studies. *J Biol Chem* 279(16):15752–15762.
3. Miksanova M, et al. (2006) Characterization of heme-regulated eIF2α kinase: Roles of the N-terminal domain in the oligomeric state, heme binding, catalysis, and inhibition. *Biochemistry* 45(32):9894–9905.
4. Hirai K, et al. (2007) Identification of Cys385 in the isolated kinase insertion domain of heme-regulated eIF2 α kinase (HRI) as the heme axial ligand by site-directed mutagenesis and spectral characterization. *J Inorg Biochem* 101(8):1172–1179.
5. Ojha S, Hwang J, Kabil O, Penner-Hahn JE, Banerjee R (2000) Characterization of the heme in human cystathionine β-synthase by X-ray absorption and electron paramagnetic resonance spectroscopies. *Biochemistry* 39(34):10542–10547.
6. Omura T, Sadano H, Hasegawa T, Yoshida Y, Kominami S (1984) Hemoprotein H-450 identified as a form of cytochrome P-450 having an endogenous ligand at the 6th coordination position of the heme. *J Biochem* 96(5):1491–1500.
7. Reynolds MF, et al. (1998) EPR and electronic absorption spectroscopies of the CO-sensing CooA protein reveal a cysteine-ligated low-spin ferric heme. *J Am Chem Soc* 120:9080–9081.
8. Aono S, Ohkubo K, Matsuo T, Nakajima H (1998) Redox-controlled ligand exchange of the heme in the CO-sensing transcriptional activator CooA. *J Biol Chem* 273(40):25757–25764.
9. Ruf HH, et al. (1984) Formation of a ferric carbanion complex from halothane and cytochrome P-450: electron spin resonance, electronic spectra, and model complexes. *Biochemistry* 23(22):5300–5306.
10. Whysner JA, Ramseyer J, Harding BW (1970) Substrate-induced changes in visible absorption and electron spin resonance properties of adrenal cortex mitochondrial P450. *J Biol Chem* 245(20):5441–5449.
11. Dawson JH, Andersson LA, Sono M (1982) Spectroscopic investigations of ferric cytochrome P-450-CAM ligand complexes. Identification of the ligand trans to cysteinate in the native enzyme. *J Biol Chem* 257(7):3606–3617.
12. Ishikawa H, et al. (2005) Involvement of heme regulatory motif in heme-mediated ubiquitination and degradation of IRP2. *Mol Cell* 19(2):171–181.

**Table S2. Statistics of the various HADDOCK docking runs**

| Scenario | HADDOCK score | $E_{electrostatic}$ | $E_{van\text{-}der\text{-}Waals}$ | Buried surface area | Cluster size best (vs. total) | Coordination* |
|---|---|---|---|---|---|---|
| WT | −53.3 ± 5.5 | −81.5 ± 54.8 | −27.9 ± 4.8 | 702.6 ± 18.0 | 51 (183) | Hexa H16:H35 |
| WT (ambiguous restraints) | −48.3 ± 1.8 | −146.2 ± 32.9 | −12.4 ± 5.3 | 575.2 ± 17.6 | 96 (176) | Penta H35 |
| H35A | −58.1 ± 2.4 | −93.5 ± 8.3 | −29.3 ± 3.8 | 637.4 ± 51.7 | 24 (180) | Penta C13 |
| H16A | −48.5 ± 2.1 | −141.1 ± 37.4 | −12.2 ± 3.8 | 603.8 ± 37.5 | 148 (196) | Penta H35 |
| C13S | −44.6 ± 3.5 | −105.4 ± 21.5 | −16.0 ± 2.3 | 588.1 ± 77.6 | 46 (183) | Penta H35 |
| C13S:H35A | −45.8 ± 7.6 | −17.1 ± 15.1 | −27.2 ± 3.7 | 669.8 ± 83.1 | 8 (178) | Penta H16 |
| C13S:H16A | −49.5 ± 3.6 | −129.4 ± 25.3 | −16.0 ± 4.7 | 616.7 ± 22.6 | 123 (188) | Penta H35 |
| H16A:H35A | −61.3 ± 2.2 | −124.3 ± 22.9 | −26.7 ± 2.6 | 715.9 ± 52.5 | 98 (185) | Penta C13 |

The program High Ambiguity Driven Protein-Protein Docking (HADDOCK) was used to generate docked structures of the complex between Pep61 or its mutants and heme. The primary sequence of Pep61 displays three residues potentially capable to be canonical binding sites for heme (C13, H16, and H35). Therefore, for the docking of the WT Pep61, the distances between the iron center of the heme and (*i*) the respective cysteine sulfur were restrained to 2.33 ± 0.05 Å, and (*ii*) distances to the two histidine ring nitrogen atoms of 1.99 ± 0.05 Å were introduced. The treatment of these restraints as ambiguous allows the program to select the preferred binding site without user-defined bias, e.g., by fulfilling only one of the three distance restraints. In addition, no further restrictions and structural assumptions were applied for the peptide backbone, i.e., also the central α-helical segment was free to evolve during the docking calculations. Docking experiments with the mutants were similarly performed with the respective adapted set of ambiguous interaction restraints.
*Iron coordination type, followed by coordinating residue(s).